Insulin regulates astrocyte gliotransmission and modulates behavior

Weikang Cai,[1] Chang Xue,[2] Masaji Sakaguchi,[1,3] Masahiro Konishi,[1] Alireza Shirazian,[4] Heather A. Ferris,[1,5] Mengyao E. Li,[1] Ruichao Yu,[6] Andre Kleinridders,[1,7,8] Emmanuel N. Pothos,[2] and C. Ronald Kahn[1]

[1]Section of Integrative Physiology and Metabolism, Joslin Diabetes Center, Harvard Medical School, Boston, Massachusetts, USA. [2]Program in Pharmacology and Experimental Therapeutics and Pharmacology and Drug Development, Sackler School of Graduate Biomedical Sciences and Department of Immunology, Tufts University School of Medicine, Boston, Massachusetts, USA. [3]Department of Metabolic Medicine, Kumamoto University, Kumamoto, Japan. [4]Public Health and Professional Degree Programs, Tufts University School of Medicine, Boston, Massachusetts, USA. [5]Division of Endocrinology and Metabolism, Department of Medicine, University of Virginia, Charlottesville, Virginia, USA. [6]Section of Pathophysiology and Molecular Pharmacology, Joslin Diabetes Center, Harvard Medical School, Boston, Massachusetts, USA. [7]German Institute of Human Nutrition Potsdam-Rehbrücke, Nuthetal, Germany. [8]National Center for Diabetes Research (DZD), Neuherberg, Germany.

Complications of diabetes affect tissues throughout the body, including the central nervous system. Epidemiological studies show that diabetic patients have an increased risk of depression, anxiety, age-related cognitive decline, and Alzheimer's disease. Mice lacking insulin receptor (IR) in the brain or on hypothalamic neurons display an array of metabolic abnormalities; however, the role of insulin action on astrocytes and neurobehaviors remains less well studied. Here, we demonstrate that astrocytes are a direct insulin target in the brain and that knockout of IR on astrocytes causes increased anxiety- and depressive-like behaviors in mice. This can be reproduced in part by deletion of IR on astrocytes in the nucleus accumbens. At a molecular level, loss of insulin signaling in astrocytes impaired tyrosine phosphorylation of Munc18c. This led to decreased exocytosis of ATP from astrocytes, resulting in decreased purinergic signaling on dopaminergic neurons. These reductions contributed to decreased dopamine release from brain slices. Central administration of ATP analogs could reverse depressive-like behaviors in mice with astrocyte IR knockout. Thus, astrocytic insulin signaling plays an important role in dopaminergic signaling, providing a potential mechanism by which astrocytic insulin action may contribute to increased rates of depression in people with diabetes, obesity, and other insulin-resistant states.

Introduction

Over the past decade it has become clear that the brain is an insulin-sensitive organ. Insulin receptors (IRs) are widely distributed in the brain (1). Intracerebroventricular insulin infusion reduces food intake and body weight from rodents to primates (2, 3). Intranasal insulin administration in healthy men has also been shown to decrease appetite and reduce body fat (4, 5). Conversely, IR deletion in the whole brain (NIRKO) leads to an array of metabolic abnormalities in mice, including increased food intake, obesity, altered response to hypoglycemia, and hypothalamic hypogonadism (6, 7). In addition, insulin action in the brain, especially in the hypothalamus, has also been shown to mediate systemic energy homeostasis by regulating peripheral metabolic tissue activities, including suppressing hepatic glucose output (8) and lipolysis in white adipose tissue (9), and by increasing thermogenesis in brown adipose tissue (10).

Although less well studied, insulin action on the brain may also modulate neurobehaviors including cognition and mood. Mice with knockout of IR in whole brain have been shown to have increased signs of depression and anxiety, especially at older ages (11). Studies also suggest that intranasal insulin administration can improve memory and mood in healthy men and women (4, 12). Conversely, individuals with diabetes and obesity have been shown to have higher rates of depression, anxiety, cognitive decline, and dementia (13–15). Many of these disorders are associated with impaired insulin signaling in the brain, even in nondiabetic individuals (16–18). While most of these effects are thought to occur through insulin action on neurons (19–21), recently it has been shown that insulin may also act on astrocytes and glial cells, affecting metabolism in both the cells themselves (22, 23) and the body as a whole (24).

Astrocytes, along with microglia and oligodendrocytes, are important for homeostasis of the brain microenvironment (25, 26). Astrocytes are responsible for the uptake of glucose and other nutrients, which will ultimately be used by energy-consuming neurons, and are part of the blood-brain barrier. Astrocytes are also responsible for uptake and degradation of excessive neurotransmitters and neuromodulators, an activity that is essential for the spatial and temporal control of neuronal activation and for avoidance of excitotoxicity. Recent studies have demonstrated that astrocytes respond to multiple stimuli to secrete neurotransmitters, like glutamate, D-serine, and ATP, in an intracellular Ca^{2+}–dependent manner, thereby actively modulating synaptic strength and neuronal activity (27–29).

In the present study, we have investigated the role of IR in the astrocytes in both whole-body energy homeostasis and neurobehaviors. We find that loss of IR in the astrocytes leads to moderate

Conflict of interest: The authors have declared that no conflict of interest exists.
Submitted: December 19, 2017; **Accepted:** April 10, 2018.
Reference information: *J Clin Invest*. 2018;128(7):2914–2926.
https://doi.org/10.1172/JCI99366.

glucose intolerance in young males. More importantly, mice lacking IR in astrocytes display increased depressive-like behavior, which is accompanied by impaired dopamine release from brain slices, particularly in the nucleus accumbens. Mechanistically, astrocytes respond to hormonal stimulation, i.e., insulin, to induce tyrosine phosphorylation of Munc18c, which activates exocytosis of ATP from astrocytes. This in turn modulates dopaminergic neuronal activity and dopamine release, which may contribute to the mood modulation in mice. Thus, insulin signaling plays an important role in astrocyte-derived purinergic signaling and thus in dopaminergic system and behavior modulation.

Results

Targeting reduction of IRs in astrocytes of intact mice. To determine the role of IR signaling in astrocytes in metabolic and neurobehavioral control, we generated mice in which the IR gene in astrocytes was inactivated by crossing mice expressing GFAP promoter–driven Cre with homozygous IR-flox ($IR^{fl/fl}$) mice to create GIRKO mice (Supplemental Figure 1A; supplemental material available online with this article; https://doi.org/10.1172/JCI99366DS1). The efficiency and specificity of GFAP-Cre–mediated recombination were confirmed using mTmG reporter mice, which showed that recombined GFP^+ cells in the brain, i.e., cells that had unique floxed allele recombination (30), also expressed the astrocyte-specific marker S100β (Supplemental Figure 1, B and C). Furthermore, when a GFAP-GFP reporter transgene was introduced into GIRKO and control $IR^{fl/fl}$ mice (Supplemental Figure 1D) and the GFP^+ cells isolated from the brain by digestion and FACS sorting, there was approximately 75% reduction of IR mRNA in GFP^+ cells from GIRKO mice compared with those from $IR^{fl/fl}$ mice (Figure 1A). At the tissue level, both mRNA and protein levels of IR were also reduced by 40% in dissected nucleus accumbens (Supplemental Figure 1, E–G), consistent with the relative abundance of astrocytes in this region. By contrast, there was no change in the expression of the insulin-like growth factor-1 receptor (IGF1R), and GIRKO mice showed a similar percentage of GFP^+ cells over total live cells as compared with the control ($IR^{fl/fl}$/GFP, 7.538% ± 0.595%, vs. GIRKO/GFP, 7.050% ± 1.104%; Figure 1B), indicating no toxicity by deletion of IR in astrocytes.

Metabolic assessment of both male and female GIRKO mice at 3 months of age revealed normal body weight, body composition, fed blood glucose, plasma insulin levels, oxygen consumption rate (VO_2), and respiratory exchange ratio (RER) (Supplemental Figures 2 and 3). Three-month-old male GIRKO mice also responded normally to exogenous insulin with a fall in blood glucose (Supplemental Figure 2F) but, consistent with a previous study (24), had slightly impaired i.p. glucose tolerance (Figure 1C). At 1 year of age, both male and female mice showed normal body weight, fasting glucose level, glucose tolerance, and insulin tolerance (Supplemental Figure 4).

Mice with astrocytic IR deletion exhibit anxiety- and depressive-like behaviors. We have previously shown that IR deletion in whole brain of mice leads to an age-dependent increase in anxiety- and depressive-like behaviors (11). This phenotype was even stronger in mice with IR knockout in astrocytes only and was marked by multiple behavioral abnormalities. Thus, female GIRKO mice showed anxiety-like behaviors as early as 4 months of age with a 60% decrease in the number of entries into the central zone in the open field test (Figure 1, D and E). This persisted at 1 year of age (Figure 1E) and was not due to defects in locomotion. Thus, young GIRKO mice traveled similar distances and at similar speeds compared with control $IR^{fl/fl}$ littermates in the open field (Supplemental Figure 5, A and B), while 1-year-old GIRKO mice traveled less distance but at the same speeds compared with $IR^{fl/fl}$ littermates (Supplemental Figure 5, C and D). Likewise, in the novelty-suppressed feeding test, overnight-fasted female GIRKO mice showed a 90% increase in the latency to feed compared with $IR^{fl/fl}$ controls (Figure 1F), consistent with increased anxiety. This occurred even though their food intake was similar to that of controls during the 1 hour after the test (Supplemental Figure 5E), indicating no alterations in hunger.

Another common indicator for altered mood and depression in rodents is anhedonia, which can be assessed using the sucrose preference test. Again, compared with $IR^{fl/fl}$ littermates, which showed a strong preference for sucrose solution over water, female GIRKO mice displayed a significantly decreased preference for sucrose (Figure 1G). Likewise, in the forced swimming test, female GIRKO mice exhibited an approximately 2-fold increase in time of immobility at both 4 months and 1 year of age (Figure 1, H and I), indicating increased depressive-like behavior. Importantly, this behavior was completely rescued by pretreatment with the antidepressant imipramine 1 hour before the test (Figure 1H), indicating that the difference in swimming was not due to defects in motor function in these mice. These differences in anxiety and depression were not driven by differences in the stress response, as indicated by similar increases in serum corticosterone levels in GIRKO mice and $IR^{fl/fl}$ littermates subjected to restraint stress (Figure 1J). Thus, loss of IR in astrocytes resulted in increased anxiety- and depressive-like behaviors in both young and aged mice. Consistent with other models showing sexual dimorphism in rodent models of anxiety and depression (31, 32), these behavioral abnormalities were strongest in female GIRKO mice. Four-month-old male GIRKO mice showed mild, nonsignificant changes in the open field, novelty-suppressed feeding, and sucrose preference tests (Supplemental Figure 6, A–D and F), but did exhibit significantly increased immobility time in the forced swimming test (Supplemental Figure 6E).

Lack of IR in astrocytes impairs dopamine release in the brain. Dopamine signaling has been linked to depression, and many antidepressants target dopamine pathways in the brain (33, 34). Indeed, we previously showed that dopamine signaling is defective in mice with a whole-brain IR knockout (NIRKO mice) (11). The nucleus accumbens (NAc), medial prefrontal cortex (mPFC), and dorsal caudate putamen (CPu) are 3 major sites that receive dopaminergic projections from the ventral tegmental area (VTA) and substantia nigra (SN) in the midbrain and are involved in mood control, reward, and movement (reviewed in ref. 35). To analyze dopamine signaling, we used carbon fiber amperometry to measure electrically evoked dopamine release in these regions from ex vivo cultured brain slices (36). We found that dopamine release in the NAc, CPu, and mPFC was decreased by about 50% in GIRKO mice compared with $IR^{fl/fl}$ littermates (Figure 2, A and B). This was due primarily to a decrease in event amplitude (Figure 2C), with no change in clearance of the released dopamine, as estimated by

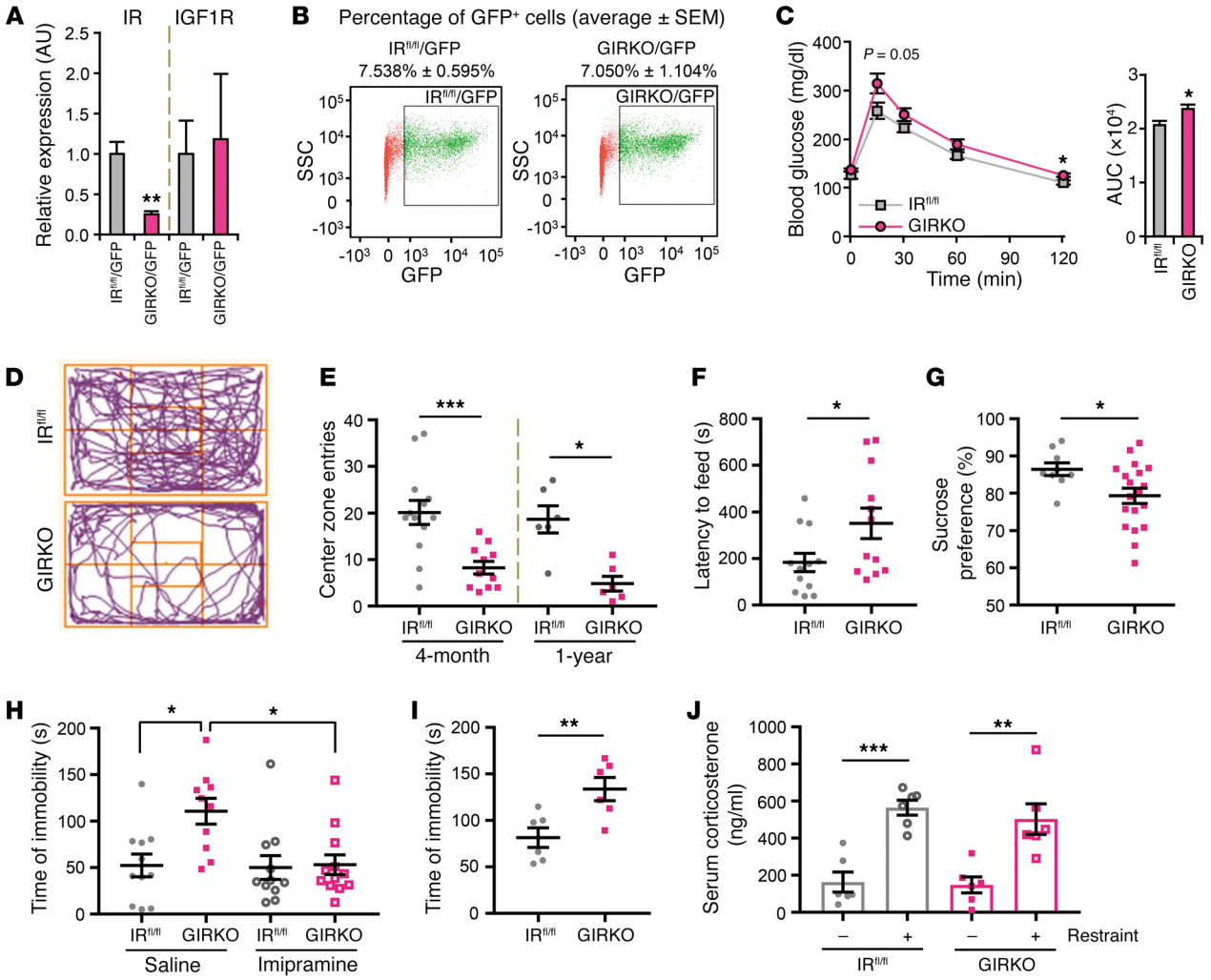

Figure 1. Loss of IR in astrocytes increases anxiety- and depressive-like behavior. (**A**) mRNA levels of IR and IGF1R from FACS-sorted astrocytes from GIRKO GFAP-GFP reporter (GIRKO/GFP, $n = 4$) and control GFAP-GFP reporter ($IR^{fl/fl}$/GFP, $n = 3$) mice normalized to TBP. $^{**}P < 0.01$, 2-tailed Student's t test. (**B**) Representative FACS profiles of cells from brains of $IR^{fl/fl}$/GFP and GIRKO/GFP mice. x axis: GFP; y axis: side-scattered light. (**C**) Glucose tolerance tests on overnight-fasted 3-month-old male $IR^{fl/fl}$ ($n = 7$) and GIRKO ($n = 6$) mice following i.p. glucose (2 g/kg). Right: Area under the curve. $^{*}P < 0.05$, 2-tailed Student's t test. (**D**) Representative movement by $IR^{fl/fl}$ and GIRKO mice in the open field. (**E**) Center zone entries of 4-month-old and 1-year-old female $IR^{fl/fl}$ and GIRKO mice in the open field test. $^{*}P < 0.05$, $^{***}P < 0.001$, 2-tailed Student's t test; 4-month-old: $IR^{fl/fl}$, $n = 13$; GIRKO, $n = 11$; 1-year-old: $n = 6$. (**F**) Latency to feeding of 4-month-old female mice in novelty-suppressed feeding test. $^{*}P < 0.05$, 2-tailed Student's t test, $n = 12$. (**G**) Sucrose preference of 4-month-old female $IR^{fl/fl}$ ($n = 9$) and GIRKO ($n = 19$) mice. $^{*}P < 0.05$, 2-tailed Student's t test. (**H**) Immobility time of 4-month-old female $IR^{fl/fl}$ and GIRKO mice in forced swimming test following saline or 16 mg/kg imipramine i.p. 1 hour before testing. $^{*}P < 0.05$, 2-way ANOVA followed by Tukey's multiple comparisons, $IR^{fl/fl}$, $n = 11$; GIRKO + saline, $n = 10$; GIRKO + imipramine, $n = 12$. (**I**) Immobility time of 1-year-old female $IR^{fl/fl}$ and GIRKO mice in forced swimming test. $^{**}P < 0.01$, 2-tailed Student's t test, $n = 6$. (**J**) Serum corticosterone of 6-month-old female $IR^{fl/fl}$ and GIRKO mice before and after 5 minutes of restraint. $^{**}P < 0.01$, $^{***}P < 0.001$, 2-tailed Student's t test, $n = 6$. All data are mean ± SEM.

rate of signal decay (Figure 2D). This also occurred with no change in total dopamine content in the brain (Figure 2E) nor change in the expression of tyrosine hydroxylase, the rate-limiting enzyme for dopamine synthesis, in the NAc, CPu, mPFC, and VTA/SN of GIRKO mice (Figure 2, F and G, and Supplemental Figure 7). In addition, the overall distribution of dopaminergic fibers and astrocytes in the NAc of GIRKO mice was similar to that in $IR^{fl/fl}$ littermates (Figure 2, H–J, and Supplemental Figure 8). mRNA expression of exocytotic vesicular monoamine transporters (VMAT1 and VMAT2) and proteins involved in dopamine uptake (DAT, Drds) and degradation (MaoA and MaoB) in the NAc, CPu, and mPFC was also comparable between GIRKO and $IR^{fl/fl}$ littermates (Figure 2G and Supplemental Figure 7). While dopamine signaling in the brain, particularly in the nigrostriatal pathway, is important for normal motor behaviors (37), both 6-month-old and 18-month-old female GIRKO mice exhibited similar stride length, grip strength, and total work on treadmill compared with control littermates (Supplemental Figure 9).

Impaired dopaminergic signaling in the NAc contributes to the depressive-like behavior in mice with astrocytic insulin signaling deficiency. To confirm that the effect of IR loss on mood behavior and dopamine signaling was on astrocyte function and not astrocyte development, we created mice with an inducible astrocyte-specific IR knockout (iGIRKO) by crossing homozygous IR-flox ($IR^{fl/fl}$)

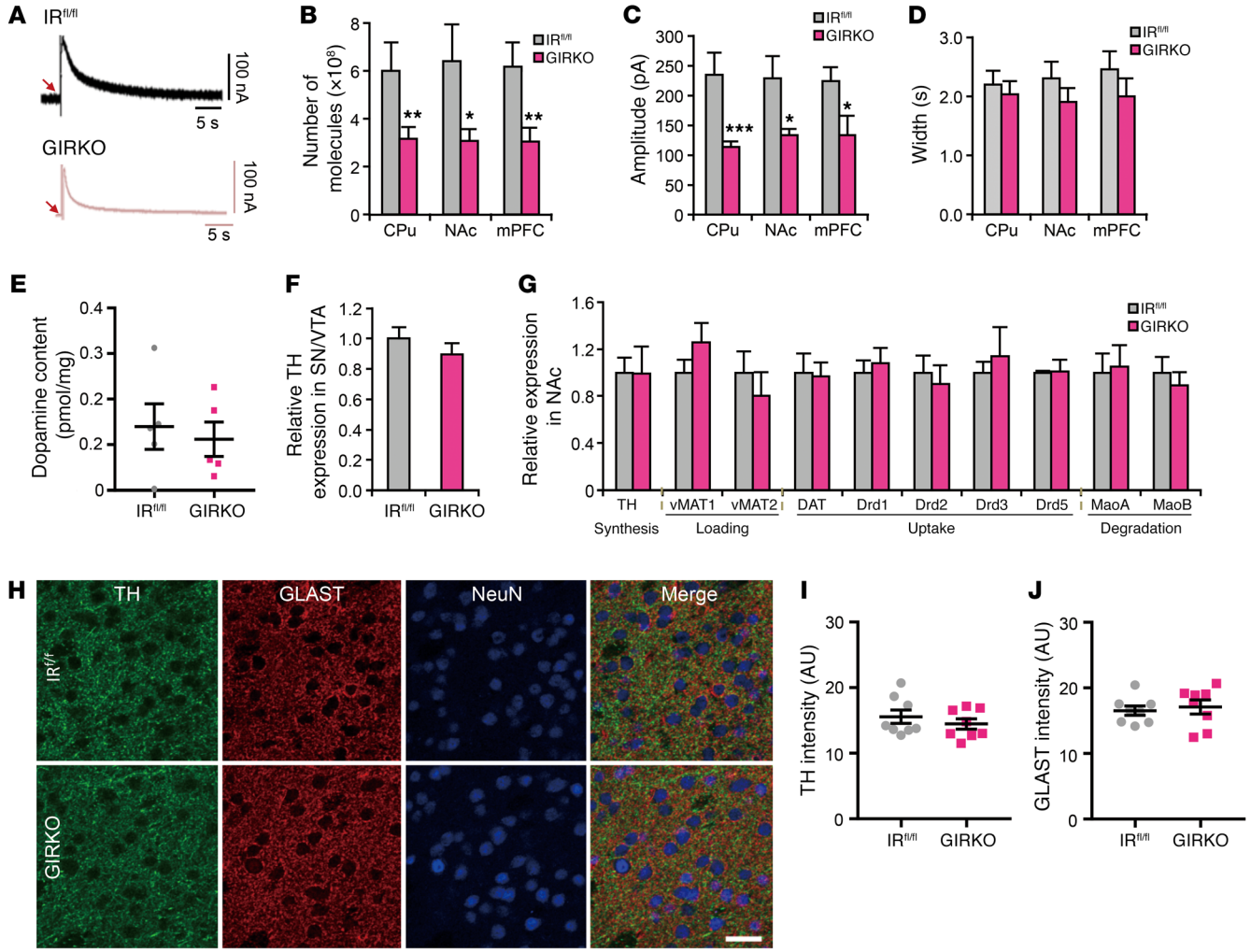

Figure 2. Loss of IR in astrocytes leads to decreased dopamine release. (**A**) Representative tracing of electrically evoked dopamine release from NAc in 3-month-old female IR$^{fl/fl}$ and GIRKO mice using carbon fiber amperometry. (**B**–**D**) Total number of dopamine molecules released (**B**), average peak amplitude of dopamine release (**C**), and average peak width (**D**) from dorsal caudate putamen (CPu), nucleus accumbens (NAc), and medial prefrontal cortex (mPFC) of 3-month-old female IR$^{fl/fl}$ and GIRKO mice. *P < 0.05, **P < 0.01, ***P < 0.001, 2-tailed Student's t test, n = 42 measurements from 19 IR$^{fl/fl}$ mice, n = 43 measurements from 19 GIRKO mice. (**E**) Total dopamine content in the brains of 3-month-old female IR$^{fl/fl}$ and GIRKO mice. n = 5, 2-tailed Student's t test. (**F**) Relative expression of tyrosine hydroxylase (TH) in the substantia nigra/ventral tegmental area (SN/VTA) of IR$^{fl/fl}$ and GIRKO mice. TBP was used as a housekeeping gene. n = 6. (**G**) Relative expression of genes involved in dopamine signaling pathways in the NAc of 3-month-old female IR$^{fl/fl}$ and GIRKO mice. TBP was used as a housekeeping gene. n = 6. (**H**) Representative images of TH/GLAST/NeuN coimmunostaining in the NAc of 4-month-old female IR$^{fl/fl}$ and GIRKO brain sections. Scale bar: 20 μm. (**I**) Mean TH intensity in the NAc of IR$^{fl/fl}$ and GIRKO brain sections. n = 8 random fields in NAc from 4 mice. (**J**) Mean GLAST intensity in the NAc of IR$^{fl/fl}$ and GIRKO brain sections. n = 8 random fields in NAc from 4 mice. All data are mean ± SEM.

mice with mice carrying GFAP-CreERT2 transgene (Figure 3A). Cre-mediated recombination in astrocytes was then induced by a series of 5 tamoxifen injections at 8 weeks of age, and recombination was confirmed 6 weeks after tamoxifen injections using mTmG reporter mice (Figure 3B and Supplemental Figure 10). IR$^{fl/fl}$ littermates given the same tamoxifen injection regimen were used as controls. Consistent with the constitutive knockout model above, female iGIRKO mice showed multiple signs of anxiety and depression, including a 33% reduction in central zone entries in the open field test (Figure 3C; P < 0.05), a significantly decreased preference for sucrose over water in the sucrose preference test (Figure 3D; P < 0.05), and a 42% increase in time of immobility in the forced swimming test compared with IR$^{fl/fl}$ littermates (Figure 3E; P < 0.05). Importantly, the increased immobility during forced swimming indicative of depressive-like behavior in iGIRKO mice was rescued by pretreatment with the specific and potent dopamine D2/D3 receptor agonist pramipexole (Figure 3E and refs. 38, 39), but not by the specific serotonin 5-HT$_{1A}$ receptor agonist 8-OH-DPAT (Figure 3F, Supplemental Figure 11, and ref. 40), indicating the importance of defective dopamine release in the depressive-like behavior in this model.

Over 95% of the neurons in the NAc express dopamine receptors (41). To further assess the downstream effect of impaired dopamine release, we assessed neuronal activation in the NAc in iGIRKO mice by c-fos immunostaining following the forced swimming test. In the control IR$^{fl/fl}$ littermates, the percentage of c-fos$^+$ neurons (i.e., c-fos$^+$ neurons/total mature NeuN$^+$ neurons) increased more than 6-fold following forced swimming. This increase in c-fos$^+$ neu-

rons was significantly blunted in iGIRKO mice, which showed only about 2-fold induction following forced swimming (Figure 3, G and H), consistent with impaired dopamine input in the iGIRKO mice.

To determine whether insulin signaling in astrocytes in either the NAc or the mPFC was important in the observed behavioral changes, we also induced site-specific deletion of IRs in astrocytes by stereotaxic injections of adeno-associated virus (AAV) encoding Cre or GFP under control of the GFAP promoter into NAc or mPFC (Figure 3I) of $IR^{fl/fl}$ mice. Interestingly, deletion of astrocytic IR in NAc, but not deletion in mPFC, caused a 30% increase in time of immobility in the forced swimming test, indicating increased depressive behavior (Figure 3, J and K). However, the astrocytic insulin signaling in NAc appears dispensable for anxiety-like behavior, since the $IR^{fl/fl}$ mice injected with AAV-GFAP-Cre showed normal center zone entries and locomotive activity in the open field test as compared with control groups receiving AAV-GFAP-GFP (Supplemental Figure 12). Thus, loss of insulin signaling in astrocytes, particularly in the NAc, results in increased depressive-like behavior in mice, which is associated with decreased dopamine release and rescued by a dopamine receptor agonist.

Insulin signaling regulates ATP release in astrocytes to modulate dopaminergic neuronal activity. To define the molecular mechanisms by which insulin signaling in astrocytes could affect dopamine release from neurons, we developed a primary cell model using astrocytes isolated from newborn $IR^{fl/fl}$ pups that could be infected with an adenovirus encoding Cre:GFP fusion protein to induce gene deletion or adenovirus-GFP as a control. In both cases, the astrocytic nature of these cells was confirmed by high expression of GFAP with no expression of the neuronal marker NeuN (Supplemental Figure 13A). As expected, the IRKO astrocytes showed almost complete loss of IR at both the mRNA and the protein level (Figure 4A and Supplemental Figure 13B). This was associated with a small and insignificant increase in the expression of the related IGF1R (Figure 4A and Supplemental Figure 13B). This was paralleled by a dramatic reduction in insulin-stimulated phosphorylation of IRS-1, Akt, ERK1/2, and GSK3 (Figure 4B). Loss of IR in the primary astrocytes also resulted in a 25%–50% decrease in expression of several proteins important in astrocyte function, including GFAP, aquaporin 4 (AQP4), glutamate transporter 1 (GLT-1), aldolase C (Aldoc), and glutamine synthetase (GS), while ApoE expression was increased by approximately 40% in the IRKO cells (Figure 4C). Expression of other astrocyte-specific proteins like glutamate aspartate transporter (GLAST), monocarboxylate transporters (MCT-1 and MCT-4), and connexin 43 (Cx43) was not changed upon IR deletion (Figure 4C).

Astrocytes can modulate neuronal activity through multiple mechanisms. Recent studies have shown that astrocytes can secrete a series of neurotransmitters, including glutamate, D-serine, and ATP, which are able to modulate activity of nearby neurons (28, 42, 43). Indeed, ATP released from astrocytes has been suggested to have anxiolytic and antidepressant effects (44). Interestingly, in control astrocytes, insulin stimulation triggered a 2-fold increase in ATP release from the culture astrocytes, and this response was completely lost in IRKO astrocytes (Figure 4D). This occurred with no change in total cellular ATP content (Figure 4E).

To assess the potential importance of ATP release by astrocytes in purinergic receptor signaling and dopamine release by neurons in the NAc, we subjected brain slices containing NAc to ex vivo electrical stimulation in the presence or absence of 2 different purinergic ligands: ATP-γ-S, a nonhydrolyzable ATP analog, and the purinergic 2 (P2) receptor agonist 2-Me-SATP. Both treatments, especially 2-Me-SATP, markedly and significantly potentiated dopamine release from NAc (Figure 4, F and G), indicating that ATP acting through the P2Y receptor is able to positively modulate dopamine release in NAc. To confirm the significance of astrocyte-derived purinergic signaling for dopamine release and depressive-like behavior in vivo, both $IR^{fl/fl}$ and iGIRKO mice were infused with 20 pmol 2-Me-SATP i.c.v. and then subjected to the forced swimming test. Again, consistent with the concept that impaired ATP release by astrocytes in iGIRKO mice was responsible for the depressive-like behaviors, 2-Me-SATP infusion decreased the time of immobility in iGIRKO mice by 50%, while the same procedure in $IR^{fl/fl}$ littermates had no significant effect (Figure 4H and Supplemental Figure 14).

Insulin signaling regulates exocytosis via tyrosine phosphorylation of Munc18c in astrocytes. Astrocytes and neurons are enriched with 2 distinct sets of SNARE proteins, which provide a foundation for differential regulation of exocytosis in these 2 cell types (45). Astrocytes highly express syntaxin-4, SNAP23, Munc18c, and VAMP3, and astrocyte-derived ATP has been shown to be dependent on SNARE complex–dependent exocytosis (44). Compared with control cells, IRKO astrocytes showed similar protein and mRNA levels of all of the astrocyte-enriched SNARE proteins, including syntaxin-4, SNAP23, VAMP3, and Munc18c, as well as the vesicular ATP transporter (VNUT) (Figure 5A). In control astrocytes, assembly of the SNARE core complex, as assessed by coimmunoprecipitation of syntaxin-4 and VAMP3, was induced more than 2-fold following insulin stimulation. By contrast, this induction was severely blunted in IRKO astrocytes (Figure 5B), despite comparable levels of intracellular Ca^{2+} (Supplemental Figure 15A) and similar expression of the 3 major inositol 1,4,5-trisphosphate receptors, ITPRs 1, 2, and 3 (Supplemental Figure 15B).

Given the role of insulin to stimulate ATP release from astrocytes, we hypothesized that the reduced ATP release from IRKO astrocytes that resulted in decreased dopaminergic neuron activation and decreased dopamine release was secondary to a loss of insulin regulation of a component of the SNARE complex. Munc18c has been shown to bind to and have an inhibitory role on syntaxin-4 (46, 47). Munc18c can be relieved of this inhibitory effect by phosphorylation at tyrosine 521, which uncovers the docking sites on syntaxin-4 for VAMP3-containing vesicles (48, 49). Consistent with the hypothesis that insulin might regulate this process, in primary control astrocytes, insulin stimulated the tyrosine phosphorylation of transfected FLAG-tagged Munc18c by 2-fold, and this induction of tyrosine phosphorylation was completely lost in IRKO astrocytes (Figure 5C). Thus, insulin stimulation of IR in astrocytes results in tyrosine phosphorylation of Munc18c. This blocks the inhibitory role of Munc18c on SNARE complex formation, allowing a stimulation of ATP release. ATP then binds to purinergic receptors on neurons, enhancing dopaminergic neuronal activity, contributing to a reduction in depression-related behaviors. In the absence of the IR, this chain of events is lost, leading to alterations in mood and behavior (Figure 6).

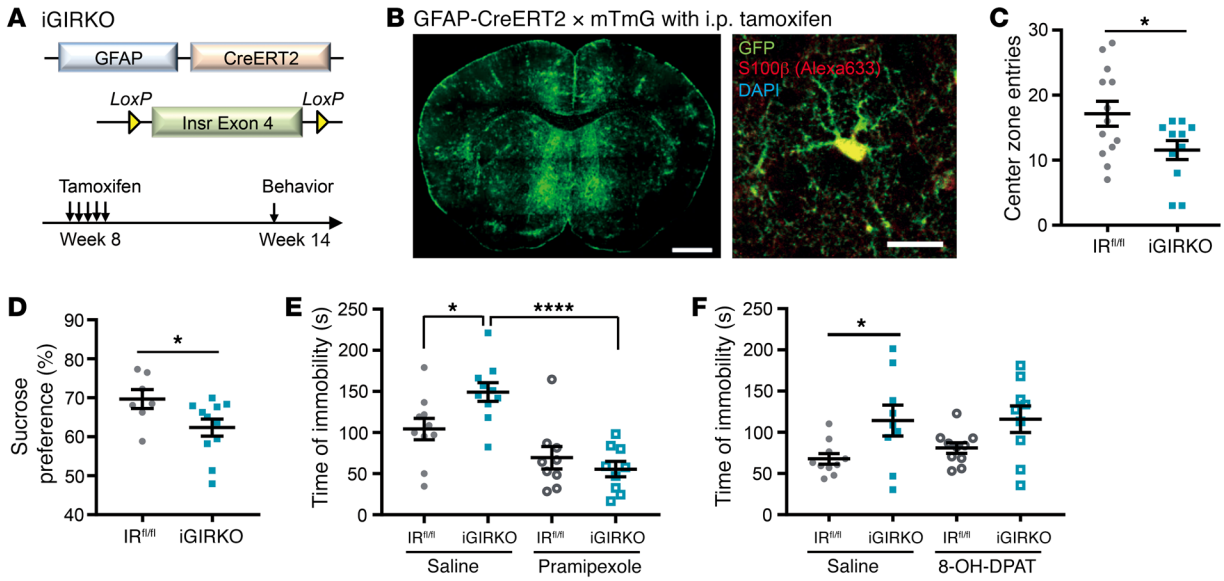

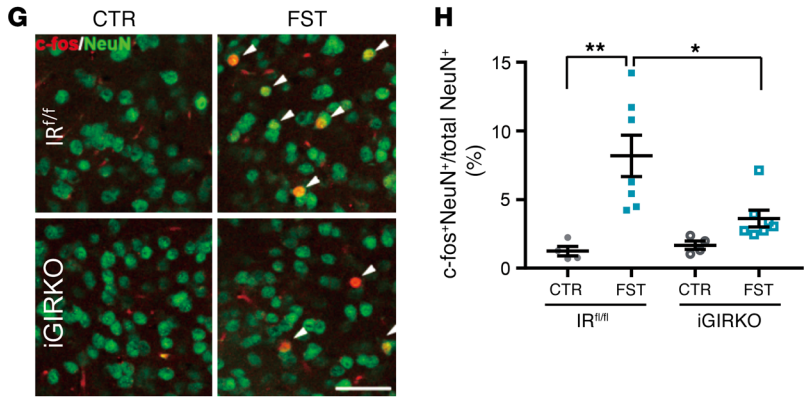

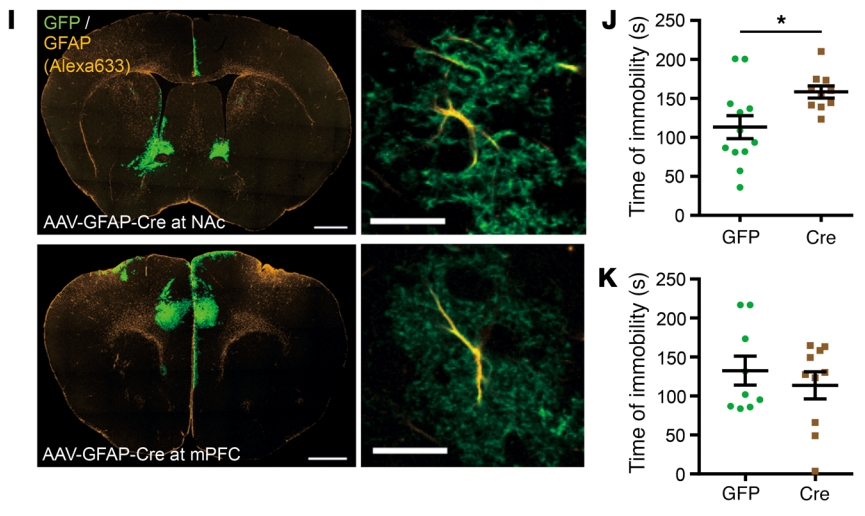

Figure 3. Deletion of IR in astrocytes in adult mice leads to depressive-like behavior. (**A**) Generation of inducible astrocyte-specific IR knockout mice. (**B**) GFP immunostaining of brain section from GFAP-CreERT2 × mTmG mouse. Scale bar: 1 mm. Right: GFP and S100β coimmunostaining in NAc. Scale bar: 20 μm. (**C**) Center zone entries of 4-month-old female $IR^{fl/fl}$ (n = 13) and iGIRKO (n = 11) mice in the open field test. *P < 0.05, 2-tailed Student's t test. (**D**) Sucrose preference of 4-month-old female $IR^{fl/fl}$ (n = 7) and iGIRKO (n = 11) mice. *P < 0.05, 2-tailed Student's t test. (**E**) Immobility time of 4-month-old female $IR^{fl/fl}$ and iGIRKO mice in forced swimming test following saline or 0.3 mg/kg pramipexole i.p. 1 hour before testing. *P < 0.05, ****P < 0.0001, 2-way ANOVA followed by Tukey's multiple comparisons, saline, iGIRKO + pramipexole, n = 10; $IR^{fl/fl}$+ pramipexole, n = 9. (**F**) Immobility time of 4-month-old female $IR^{fl/fl}$ (n = 10) and iGIRKO (n = 9) mice in forced swimming test following saline or 0.3 mg/kg 8-OH-DPAT i.p. 1 hour before testing. *P < 0.05, repeated 2-way ANOVA followed by Sidak's multiple comparisons. (**G**) c-fos (red) and NeuN (green) coimmunostaining in NAc of $IR^{fl/fl}$ and iGIRKO mice basally (CTR) and 1 hour after forced swimming test (FST). Scale bars: 50 μm. (**H**) Quantification of c-fos$^+$ neurons *P < 0.05, **P < 0.01, 2-way ANOVA followed by Tukey's multiple comparisons, CTR, n = 4; FST, n = 7. (**I**) GFP and GFAP coimmunostaining on a brain sections from an mTmG mouse injected with AAV-GFAP-Cre in NAc (top) and mPFC (bottom). Scale bars: 1 mm. Right: Colocalization of GFP and GFAP in an astrocyte. Scale bars: 20 μm. (**J** and **K**) Immobility time in the forced swimming test of 4-month-old female $IR^{fl/fl}$ mice injected with AAV-GFAP-Cre or GFP in NAc (**J**) or mPFC (**K**). *P < 0.05, 2-tailed Student's t test. NAc: GFP, n = 12; Cre, n = 10; mPFC: GFP, n = 9, Cre, n = 10. All data are mean ± SEM.

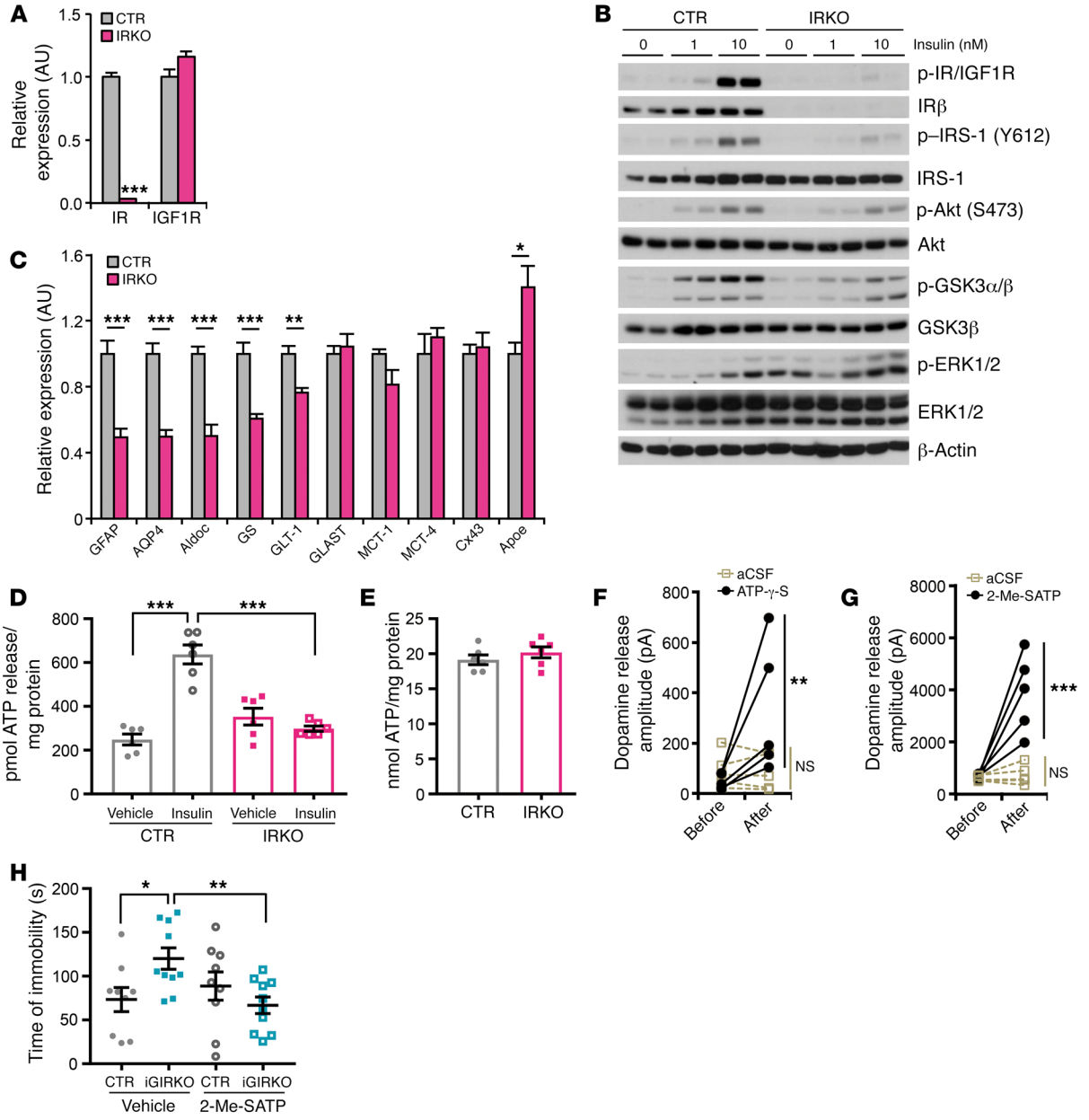

Figure 4. IR in astrocytes regulates ATP exocytosis to modulate dopamine release. (**A**) mRNA expression of IR and IGF1R in primary $IR^{fl/fl}$ astrocytes infected with adenovirus encoding Cre or GFP. TBP was used as a housekeeping gene. ***$P < 0.001$, 2-tailed Student's t test, $n = 6$. (**B**) Immunoblotting of phosphorylation of insulin signaling molecules in CTR and IRKO astrocytes following indicated concentrations of insulin stimulation for 10 minutes. (**C**) Relative expression of astrocyte-specific markers in CTR and IRKO astrocytes. TBP was used as a housekeeping gene. *$P < 0.05$, **$P < 0.01$, ***$P < 0.001$, 2-tailed Student's t test, $n = 6$. (**D**) ATP release from CTR and IRKO astrocytes in the presence or absence of 100 nM insulin stimulation for 30 minutes. ***$P < 0.001$, 2-tailed Student's t test, $n = 6$. (**E**) Total ATP content in both CTR and IRKO astrocytes. $n = 6$. (**F**) Peak amplitude of electrically evoked dopamine release from NAc before and after infusion of aCSF or ATP-γ-S. **$P < 0.01$ vs. basal, repeated 2-way ANOVA followed by Sidak's multiple comparisons, $n = 5$. (**G**) Peak amplitude of electrically evoked dopamine release from NAc before and after infusion of aCSF or 2-Me-SATP. ***$P < 0.001$ vs. basal, repeated 2-way ANOVA followed by Sidak's multiple comparisons, $n = 5$. (**H**) Time of immobility of 4-month-old female $IR^{fl/fl}$ CTR and iGIRKO mice in forced swimming test with i.c.v. infusion of saline or 20 pmol 2-Me-SATP 1 hour before the test. *$P < 0.05$, **$P < 0.01$, 2-way ANOVA followed by Sidak's multiple comparisons, $n = 9$ for CTR groups, $n = 10$ for iGIRKO groups. All data are mean ± SEM.

Discussion

While the brain has been classically regarded as an insulin-insensitive tissue, many recent studies have shown that this is not the case. Indeed, insulin action on the brain has been shown to regulate feeding, hepatic glucose output, body temperature, and energy homeostasis, as well as other metabolic and endocrine functions (reviewed in ref. 1). These defects have been thought to be mediated predominantly by insulin action on neurons, although we and others have shown that insulin acting on glial cells can regulate cholesterol synthesis (22) and alter some aspects of whole-body metabolic control (24). In the present study, using 2 genetically engineered mouse models, as well as primary cells, we

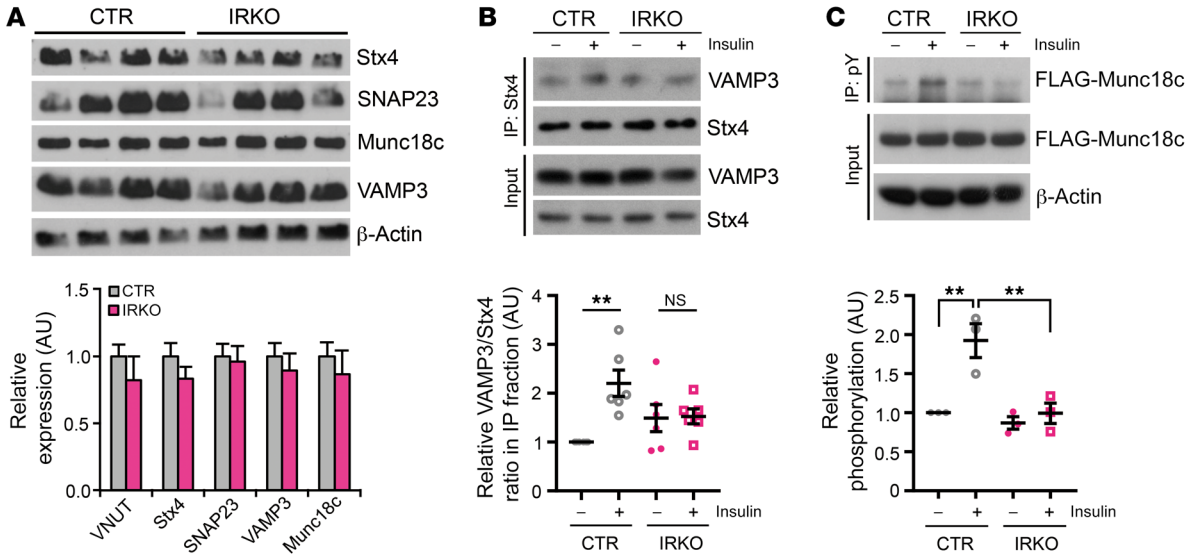

Figure 5. IR in astrocytes regulates exocytosis through Munc18c tyrosine phosphorylation. (**A**) Top: Immunoblotting of astrocyte-enriched SNARE complex proteins in CTR and IRKO astrocytes. Bottom: Relative mRNA expression of astrocyte-enriched SNARE complex proteins and vesicular ATP transporter VNUT in CTR and IRKO astrocytes. TBP was used as a housekeeping gene. $n = 6$. (**B**) Top: Coimmunoprecipitation showing syntaxin-4 (Stx4)/VAMP3 interaction in CTR and IRKO astrocytes in the basal state and after insulin stimulation (100 nM, 30 minutes). Bottom: Densitometry analysis showing impaired Stx4/VAMP3 interaction in IRKO astrocytes following insulin stimulation. $^{**}P < 0.01$, 2-way ANOVA followed by Tukey's multiple comparisons, $n = 6$. (**C**) Top: Tyrosine phosphorylation of FLAG-Munc18c in CTR and IRKO astrocytes in the basal state and after insulin stimulation (100 nM, 30 minutes). Bottom: Densitometry analysis showing loss of insulin-stimulated Munc18c tyrosine phosphorylation in IRKO astrocytes. $^{**}P < 0.01$, 2-way ANOVA followed by Tukey's multiple comparisons, $n = 3$. All data are mean ± SEM.

demonstrate that insulin signaling in astrocytes plays a crucial role in potentiating release of dopamine and that loss of this function has important effects on regulation of mood and behavior.

Diabetes is associated with a number of CNS abnormalities, including increased risks of cognitive impairment, Alzheimer's disease, anxiety, and depression (50, 51). Impaired signaling downstream of the IR has been demonstrated in brains from patients with Alzheimer's disease even in the absence of diabetes (17). Mice with knockout of IR in all cells of the brain have been shown to display anxiety- and depressive-like behaviors as they age (11). Likewise, mice with insulin resistance secondary to diet-induced obesity (52) or genetic defects (53) display anxiety- and depressive-like behaviors. Conversely, systemic insulin delivery has been shown to have an antidepressant effect in diabetic mice (54), and some studies have suggested that insulin can slow the rate of cognitive decline in patients with Alzheimer's disease (55) and even have beneficial effects on mood and cognition in healthy subjects (12). The present study demonstrates that insulin signaling in astrocytes is critical for mood control. Indeed, loss of IRs on astrocytes in the NAc is sufficient to induce depressive-like behavior in mice, demonstrating the importance of astrocytic insulin signaling in behavioral control.

IRs are expressed on both neurons and glial cells. The action of insulin in neurons in the arcuate nucleus of the hypothalamus has been shown to inhibit orexigenic AgRP/NPY neurons, while activating anorexigenic proopiomelanocortin (POMC) neurons (20, 56). As a result, modulation of these neuronal populations by insulin suppresses food intake. In addition, the action of insulin on AgRP neurons has been shown to be critical for suppression of hepatic glucose production (19), while its action on POMC neurons controls adipose tissue lipolysis (21). Hypothalamic IRs have also been shown to be important for the regulation of thermogenesis and reproductive fertility (6, 57). The effects of insulin signaling, however, are not limited to hypothalamic neurons, since insulin has also been shown to act on cholinergic interneurons in striatum to potentiate the reward response (58).

The present study demonstrates that besides neurons, astrocytes are an important insulin-responsive element in the brain. Thus, insulin acutely stimulates astrocyte exocytosis by phosphorylation of Munc18c on tyrosine residues, alleviating its inhibitory effect on syntaxin-4. This results in increased release of ATP and possibly other gliotransmitters and metabolites from astrocytes, which can modulate the activity of dopaminergic neurons and potentially other neurons (i.e., serotonergic neurons). In this regard, the regulation of the syntaxin-4/Munc18c complex in astrocytes is similar to that in peripheral insulin-sensitive tissues, such as adipose tissue and muscle, where Munc18c has been shown to be involved in insulin-stimulated translocation of intracellular GLUT4-containing vesicles to the plasma membrane (48, 59, 60). This enrichment of syntaxin-4/Munc18c in astrocytes, but not neurons, provides a unique mechanism by which insulin can specifically target astrocytes in the central nervous system.

This acute action of insulin on astrocytes is in addition to more chronic effects of insulin on cellular metabolism. For example, we and others have shown that insulin regulates cholesterol synthesis in astroglial cells (22), and this astrocyte-derived cholesterol is released from astrocytes complexed to ApoE-containing lipoproteins, which can then be taken up by neurons where the cholesterol participates in membrane homeostasis and synaptic remodeling (61). Somewhat paradoxically, we find that ApoE mRNA is increased

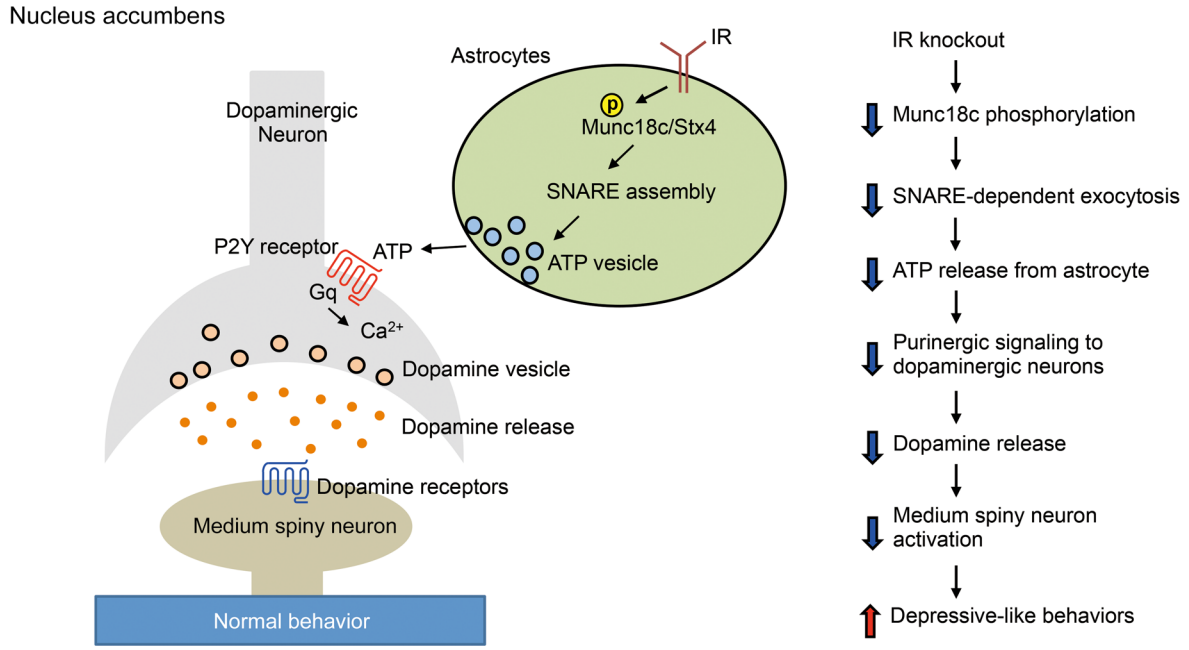

Figure 6. Proposed model of astrocytic insulin signaling in the regulation of dopaminergic neuronal activity and behavior. Left: Insulin activates IR on astrocytes to induce syntaxin-4 (Stx4):Munc18c SNARE complex–dependent ATP exocytosis, which contributes to the modulation of dopaminergic neuronal activity and mood behavior. Right: Loss of IR in astrocytes results in dysregulation of the proposed signaling pathway, leading to depressive-like behavior.

in the astrocytes lacking IR, suggesting that at the level of gene expression, insulin signaling suppresses ApoE expression in the astrocytes. Since ApoEε is the most significant risk allele for Alzheimer's disease (62), the impact of insulin regulation on ApoE in Alzheimer's disease requires further investigations. Others have found that loss of IRs in astrocytes can also result in decreased expression of GLUT1 and increased expression of carnitine palmitoyltransferase 1C (CPT1C), shifting the fuel preference of the astrocytes from glucose to lipids and changing mitochondria oxidation (24). Thus, insulin can regulate multiple aspects of astrocyte function, which can modulate neuronal plasticity and activity in the brain.

While our study focuses on the role of insulin in astrocytes, astroglial dysfunction can occur in individuals with mental illness, even in the absence of diabetes. Histopathological studies have shown that glial cell density is reduced in the prefrontal cortex, hippocampus, and amygdala of patients with major depressive disorders and that this is associated with alterations in the expression of astrocyte-specific markers (reviewed in refs. 63, 64). Treatment with antidepressants might also indirectly alter IR expression and signaling through effects on structural proteins, receptor expression, and activation of intracellular pathways in astrocytes (reviewed in ref. 65). The present study demonstrates that insulin-dependent release of ATP from astrocytes is critical for normal mood control. This is supported by other studies showing that ATP levels are decreased in many brain regions in rodent models of depression (44) and that a P2Y1 receptor agonist can cause anxiolytic effects in the rat (66).

Our data indicate that the dopamine system may be an important mechanistic link between astrocytic insulin action and mood regulation, since selective dopamine D2/D3 receptor agonist, but not serotonin 5-HT_{1A} receptor agonist, acutely reversed the depressive-like behavior in mice lacking IR in astrocytes. However, this does not rule out the possibility that astrocytic insulin signaling–mediated ATP release may have effects on other neural systems, including the serotonin and cannabinoid systems (67, 68), to modulate mood behaviors in mice. For example, impaired serotonin signaling may play a role in the depressive-like behavior in these mice by modulating dopaminergic neuronal activity through other serotonin receptor subtypes like 5-HT_{2C} (69). In addition to dopaminergic neurons, modulation of neuronal activity by astrocyte-derived "gliotransmitters" has also been reported in hippocampal pyramidal neurons through effects of glutamate (42) and in hypothalamic AgRP neurons through the action of AMP (70, 71). Whether insulin signaling–dependent gliotransmission from astrocytes plays a significant role in other neural circuits awaits further investigations.

In summary, we have demonstrated that astrocytes are an important target for insulin signaling in control of mood and behavior. Astrocytic insulin signaling regulates Munc18c phosphorylation and syntaxin-4–dependent ATP exocytosis, which in turn modulates presynaptic dopaminergic neuronal activity and dopamine release. Thus, astrocytic IR–deficient mice exhibit impaired dopamine release in brain slices and increased depressive-like behaviors. Developing new agents to target this aspect of astrocyte biology could provide a novel approach to the treatment of mood and behavioral disorders in both diabetic and nondiabetic individuals.

Methods

Animal models. Mice were housed in standard cages with a 12-hour light/12-hour dark cycle and fed a 22% fat chow diet (Mouse Diet 9F, LabDiet). Both male and female mice were used as indicated. All animal studies were approved by the IACUCs at Joslin Diabetes Center and

Tufts University and were in accordance with NIH guidelines. Additional information about animal studies is given in Supplemental Methods.

Behavioral assessment. Male and female (4-month-old and 1-year-old) mice were used for behavioral tests. Each mouse was exposed to each specific behavioral test only once in its lifetime unless otherwise indicated. Only 1 behavioral test was performed per week to minimize the stress. All mice were transferred to the behavioral testing room the day before the test for acclimation.

In the open field test, each mouse was placed in an open box 57 × 37 × 31 cm. During the 5-minute session, the movement of the mouse was recorded with an HD webcam and analyzed by ANY-maze software (Stoelting Co.). Central zone entries, total distance traveled, and maximum speed were measured.

For the novelty-suppressed feeding test, mice were fasted overnight (16 hours). Each mouse was placed in a well-illuminated open field box (57 × 37 × 31 cm) with a white 15-cm disc containing a food pellet in the center of the box. The movement of the mouse was recorded for maximum 15 minutes and analyzed by ANY-maze software. The latency to feeding and food intake by each mouse in a housing cage in the hour immediately following testing were measured.

In the forced swimming test, each mouse was placed in a vertical Plexiglas cylinder (40 cm height, 18 cm diameter) containing water 15 cm deep (23°C–25°C). The mouse was allowed to swim inside the cylinder and videotaped for 6 minutes. Videos were analyzed by ANY-maze software. During the testing period, the total time of immobility was assessed as a measure of "despair" or depression. In the same studies, the antidepressant imipramine (16 mg/kg; Sigma-Aldrich), the dopamine D2/D3 receptor agonist pramipexole (0.3 mg/kg; Sigma-Aldrich), or the serotonin 5-HT_{1A} receptor agonist 8-OH-DPAT (0.3 mg/kg; Tocris) was injected i.p. into a subgroup of GIRKO or iGIRKO mice and $IR^{fl/fl}$ littermates 1 hour before the test.

In the sucrose preference test, mice were single-housed and habituated for 24 hours in the behavioral testing room with both bottles containing water. After habituation, the mouse was given free access to 2 water bottles: one containing 1% sucrose solution and the other plain water. Daily water and sucrose intake was measured for the next 4 days. The placement of water and sucrose bottles was switched each day to avoid memory-driven behavior. Sucrose preference was presented as the percentage of the volume of sucrose intake over the volume of total fluid intake.

Brain slice preparation. Eleven- to twelve-week-old female mice fed normal chow were euthanized using a ketamine-xylazine cocktail. The brain was placed in ice-cold oxygenated sucrose bicarbonate solution (210 mM sucrose, 10 mM glucose, 3.5 mM KCl, 1 mM $CaCl_2$, 4 mM $MgCl_2$, 1.25 mM NaH_2PO_4). The 2 halves of the neocortex were promptly glued to a metallic base fitting a Leica VT1000S Vibratome (Leica Microsystems) and cut in 300-μm coronal brain slices, which were transferred to a container filled with oxygenated aCSF (124 mM NaCl, 2 mM KCl, 1.25 mM KH_2PO_4, 2 mM $MgSO_4$, 25 mM $NaHCO_3$, 2 mM $CaCl_2$, and 11 mM glucose) at room temperature. Brain slices were allowed to recover for an hour after dissection. Slices with the 3 sites that contain the bulk of terminals projecting from the dopaminergic midbrain (prefrontal cortex, NAc, or CPu) were used for testing.

Dopamine release measured by carbon fiber amperometry. Amperometric electrodes were 5-μm carbon fibers (Amoco). The electrodes were back-filled with 3 M KCl and beveled at the tip. Electrode response was tested by cyclic voltammetry. A positive 700-mV voltage (vs. an Ag-AgCl ground) was applied to the carbon fiber electrode using a 200B amplifier (Axon Instruments). The amperometric electrode was placed in the prefrontal cortex, dorsal striatum, or NAc. A bipolar stimulating electrode (PlasticsOne) was placed 100–200 μm away from the carbon fiber electrode. A current stimulus of +500 μA was applied 5 times per site every 5 minutes for 2 milliseconds. The response of the amperometric electrode (increase above baseline) was recorded using Axograph. The output was digitized at 50 kHz, low-pass-filtered at 1 kHz, and analyzed using Axograph. The number of molecules oxidized was determined by the relation $N = Q/nF$, where Q is the charge of the spike, n is the number of electrons transferred (2 for catecholamines), N is the number of moles, and F is Faraday's constant (96,485 coulombs per unit charge).

To test the role of purinergic signaling in dopamine release, 2 slices that contained NAc were used for each mouse; 5 mice were used in total. Electrically evoked dopamine release from 1 slice was measured in oxygenated aCSF, and measured again following incubation with either 150 μM ATP-γ-S for 10 minutes or 10 μM 2-Me-SATP for 40 minutes. The other slice was subjected to the same procedure with oxygenated aCSF for the same time period as the experimental slice.

Measurement of dopamine content by HPLC. Whole brains from 3-month-old GIRKO mice and $IR^{fl/fl}$ littermates were rinsed in aCSF solution to remove blood and homogenized in 1 ml 0.3 M perchloric acid. Lysates were repeatedly sonicated (1 minute) and frozen on dry ice (10 minutes) 3 times. The samples were spun for 25 minutes at 135 *g*, the supernatant collected, and total volume measured. Twenty microliters supernatant from each sample was injected into an HPLC system coupled to an electrochemical detector (Antec INTRO) with the GBC LC1120 HPLC pump pressure of 1,200 psi. The total amounts of dopamine and other neurotransmitters were measured. The pellets were solubilized in 1× RIPA buffer with protease inhibitor cocktail (Calbiochem) by sonication. Protein concentrations, measured using the bicinchoninic acid (BCA) protein assay, were used for normalization.

Stereotaxic injections. $IR^{fl/fl}$ mice were anesthetized with a ketamine (100 mg/ml) and xylazine (20 mg/ml) mix diluted in saline and placed into a stereotaxic station (Kopf Instruments). The skull was exposed via a small incision, and a small hole was drilled to the desired coordinates for viral injection. A 33-gauge needle (Hamilton) was inserted bilaterally into the NAc (from bregma: anterior–posterior, +1.2 mm; medial–lateral, ±2.5 mm; dorsal–ventral, –4.8 mm; angle, ±18%) and mPFC (from bregma: anterior–posterior, +2.0 mm; medial–lateral, ±0.4 mm; dorsal–ventral, –2.5 mm). One microliter (2×10^8 viral genome particles) AAV-DJ/8-GFAP-Cre:GFP or GFP-only viruses were injected bilaterally into NAc or mPFC using a 2.5-μl Hamilton microsyringe. The needle was withdrawn 5 minutes after the injection.

Intracerebroventricular injection. Both 13-week-old $IR^{fl/fl}$ and iGIRKO female mice were anesthetized with a ketamine (100 mg/ml) and xylazine (20 mg/ml) mix diluted in saline and placed into a stereotaxic station (Kopf Instruments). A stainless steel guide cannula (PlasticsOne) with 2 mm guide length was implanted into the lateral cerebral ventricle. The stereotaxic coordinates were –0.5 mm posterior and +1.0 mm lateral from bregma. Correct placement of the cannula was verified by i.c.v. injection of angiotensin II (1 μg in 1 μl 0.9% saline; Sigma-Aldrich) 3 days after the cannula implantation. Mice that failed to consume water within 30 minutes after the injections were removed from the following study. One week after the implantation, mice were injected with 2 μl saline or 2-Me-SATP (10 μM) i.c.v. in a randomized

fashion 1 hour before the forced swimming test. One group of mice were given saline followed by forced swimming test at week 1 and then given 2-Me-SATP followed by forced swimming test at week 2. In the second group of mice the order of tests was reversed.

Primary astrocyte culture. Primary cultures of cortical astrocytes were prepared from $IR^{fl/fl}$ newborn pups. Both cortices were surgically dissected in ice-cold Hybernate A medium (Invitrogen). After the removal of meninges, the cortical tissues were dissociated by treatment for 30 minutes at 37°C in Hybernate A supplemented with 4 mg/ml papain (Sigma-Aldrich) and 0.0025 mg/ml DNase I (Sigma-Aldrich), subjected to gentle trituration in DMEM plus 10% FBS, and plated on 75 cm^2 cell culture flasks. Following incubation overnight in a humidified incubator at 37°C and 5% CO_2, the flasks were vigorously shaken to detach neurons and microglia. Culture medium (DMEM supplemented with 10% FBS, 100 U/ml penicillin, and 100 μg/ml streptomycin) was replaced every 3 days thereafter until the cell monolayer reached confluence.

ATP release assay. Cells cultured in 12-well plates were washed twice with 1× HBSS and serum-starved in HBSS for an additional 4 hours. After the starvation period, the medium was replaced with 1× HBSS plus 100 μM ARL67156 (an ecto-ATPase inhibitor) with or without 100 nM insulin. After 30 minutes of incubation, the supernatant was collected, and ATP quantitated using a luciferase-based ATP determination kit (Thermo Fisher Scientific). Cells were lysed with RIPA lysis buffer complemented with 50 mM KF, 50 mM β-glycerolphosphate, 2 mM EGTA (pH 8), 1 mM Na_3VO_4, and 1× protease inhibitor cocktail (Calbiochem). Protein concentrations were determined using the Pierce 660 nm Protein Assay Reagent (Thermo Fisher Scientific) and used for normalization.

To quantify the total ATP content in the cells, 50 μl of cell lysates were mixed with 50 μl 2 M perchloric acid by vortexing and incubated on ice for 5 minutes. After centrifugation, the supernatant was mixed with 50 μl 3 M KOH, vortexed, and centrifuged to precipitate the remaining perchloric acid. The resultant supernatant was neutralized using HCl and subjected to ATP assay as described above.

Munc18c tyrosine phosphorylation. Both control and IRKO astrocytes were infected with adenovirus encoding FLAG-tagged Munc18c (1×10^9 genomic copies/ml) for 24 hours. The cells were cultured for an additional 5 days before the experiment. Cells were serum-starved in DMEM plus 0.1% BSA for 5 hours before 10 nM insulin stimulation for 15 minutes. After stimulation, cells were washed immediately with ice-cold PBS once and lysed in lysis buffer (20 mM HEPES [pH 7.4], 150 mM NaCl, 50 mM KF, 50 mM β-glycerolphosphate, 2 mM EGTA [pH 8], 1 mM Na_3VO_4, 1% Triton X-100, 10% glycerol, and 1× protease inhibitor cocktail [Calbiochem]). Protein concentrations were determined using the Pierce 660 nm Protein Assay Reagent (Thermo Fisher Scientific). To immunoprecipitate total phosphotyrosine-containing proteins, 600 μg protein lysates were incubated with 1 μg anti-phosphotyrosine antibody (Santa Cruz Biotechnology) in a total volume of 800 μl overnight at 4°C with end-to-end rotation, followed by a 1-hour incubation with 20 μl protein A/G–conjugated magnetic beads at 4°C with end-to-end rotation. The immunocomplexes were pulled down with a magnetic rack and washed sequentially: 1 time with lysis buffer, 2 times with lysis buffer plus 500 mM NaCl, and 2 times with lysis buffer. Bound proteins were eluted by incubation for 5 minutes at 100°C in 1× SDS loading buffer. The bound proteins along with 10 μg total cell lysates from each sample were resolved using SDS-PAGE and transferred to PVDF membranes. The level of Munc18c tyrosine phosphorylation was assessed by immunoblotting using anti-FLAG antibodies (Sigma-Aldrich). See complete unedited blots in the supplemental material.

Statistics. All the data are presented as mean ± SEM. Two groups were compared using unpaired 2-tailed Student's *t* test. Two-way ANOVA was performed to detect the interactions between genotype and treatment (i.e., insulin, antidepressants, receptor agonists, restraint), and Tukey's post hoc analysis was performed when appropriate. Repeated 2-way ANOVA was performed to detect the significant interaction between treatment and genotype followed by Sidak's multiple comparisons. A *P* value less than 0.05 was considered significant.

Study approval. All animal studies were approved by the IACUCs of Joslin Diabetes Center, Boston, Massachusetts, USA, and Tufts University School of Medicine, Boston, Massachusetts, USA, and were in accordance with NIH guidelines.

Author contributions

WC designed the study, researched data, and wrote the manuscript. CX, MS, MK, AS, HAF, MEL, RY, AK, and ENP researched data and helped design experiments. CRK designed the study, supervised all work, and helped write the manuscript.

Acknowledgments

This work was supported by NIH grants R01 DK031036 and R01 DK033201 (to CRK) and R01 DK065872 (to ENP). The work was also supported by the Boston University/Joslin Diabetes Center Pilot and Feasibility Award (to ENP), and Tufts Center for Neuroscience Research P30 NS047243. MS was supported by the MSD Life Science Foundation and the Takeda Science Foundation. HAF was supported by NIH grant 5 K08 DK097293. AK was supported by Deutsche Forschungsgemeinschaft grant project KL 2399/4-1 and the Federal Ministry of Education and Research (German Center for Diabetes Research, grant 01GI092). The Joslin Diabetes Center DRC Advanced Microscopy Core, Flow Cytometry Core, and Animal Physiology Core (P30 DK036836) also provided important help.

Address correspondence to: C. Ronald Kahn, Joslin Diabetes Center, 1 Joslin Place, Boston, Massachusetts 02215, USA. Phone: 617.732.2635; Email: c.ronald.kahn@joslin.harvard.edu.

1. Kleinridders A, Ferris HA, Cai W, Kahn CR. Insulin action in brain regulates systemic metabolism and brain function. *Diabetes*. 2014;63(7):2232–2243.
2. Florant GL, Singer L, Scheurink AJ, Park CR, Richardson RD, Woods SC. Intraventricular insulin reduces food intake and body weight of marmots during the summer feeding period. *Physiol Behav*. 1991;49(2):335–338.
3. Woods SC, Lotter EC, McKay LD, Porte D. Chronic intracerebroventricular infusion of insulin reduces food intake and body weight of baboons. *Nature*. 1979;282(5738):503–505.
4. Benedict C, Kern W, Schultes B, Born J, Hallschmid M. Differential sensitivity of men and women to anorexigenic and memory-improving effects of intranasal insulin. *J Clin Endocrinol Metab*. 2008;93(4):1339–1344.
5. Hallschmid M, Benedict C, Schultes B, Fehm HL, Born J, Kern W. Intranasal insulin reduces body fat in men but not in women. *Diabetes*. 2004;53(11):3024–3029.

6. Brüning JC, et al. Role of brain insulin receptor in control of body weight and reproduction. *Science*. 2000;289(5487):2122–2125.
7. Fisher SJ, Brüning JC, Lannon S, Kahn CR. Insulin signaling in the central nervous system is critical for the normal sympathoadrenal response to hypoglycemia. *Diabetes*. 2005;54(5):1447–1451.
8. Obici S, Zhang BB, Karkanias G, Rossetti L. Hypothalamic insulin signaling is required for inhibition of glucose production. *Nat Med*. 2002;8(12):1376–1382.
9. Scherer T, et al. Brain insulin controls adipose tissue lipolysis and lipogenesis. *Cell Metab*. 2011;13(2):183–194.
10. Sanchez-Alavez M, et al. Insulin causes hyperthermia by direct inhibition of warm-sensitive neurons. *Diabetes*. 2010;59(1):43–50.
11. Kleinridders A, et al. Insulin resistance in brain alters dopamine turnover and causes behavioral disorders. *Proc Natl Acad Sci U S A*. 2015;112(11):3463–3468.
12. Benedict C, et al. Intranasal insulin improves memory in humans. *Psychoneuroendocrinology*. 2004;29(10):1326–1334.
13. Blázquez E, Velázquez E, Hurtado-Carneiro V, Ruiz-Albusac JM. Insulin in the brain: its pathophysiological implications for States related with central insulin resistance, type 2 diabetes and Alzheimer's disease. *Front Endocrinol (Lausanne)*. 2014;5:161.
14. Kopf D, Frölich L. Risk of incident Alzheimer's disease in diabetic patients: a systematic review of prospective trials. *J Alzheimers Dis*. 2009;16(4):677–685.
15. Eaton WW, Armenian H, Gallo J, Pratt L, Ford DE. Depression and risk for onset of type II diabetes. A prospective population-based study. *Diabetes Care*. 1996;19(10):1097–1102.
16. Craft S. Insulin resistance syndrome and Alzheimer's disease: age- and obesity-related effects on memory, amyloid, and inflammation. *Neurobiol Aging*. 2005;26(suppl 1):65–69.
17. Talbot K, et al. Demonstrated brain insulin resistance in Alzheimer's disease patients is associated with IGF-1 resistance, IRS-1 dysregulation, and cognitive decline. *J Clin Invest*. 2012;122(4):1316–1338.
18. Liu Y, Liu F, Grundke-Iqbal I, Iqbal K, Gong CX. Deficient brain insulin signalling pathway in Alzheimer's disease and diabetes. *J Pathol*. 2011;225(1):54–62.
19. Könner AC, et al. Insulin action in AgRP-expressing neurons is required for suppression of hepatic glucose production. *Cell Metab*. 2007;5(6):438–449.
20. Loh K, et al. Insulin controls food intake and energy balance via NPY neurons. *Mol Metab*. 2017;6(6):574–584.
21. Shin AC, et al. Insulin receptor signaling in POMC, but not AgRP, neurons controls adipose tissue insulin action. *Diabetes*. 2017;66(6):1560–1571.
22. Suzuki R, et al. Diabetes and insulin in regulation of brain cholesterol metabolism. *Cell Metab*. 2010;12(6):567–579.
23. Heni M, et al. Insulin promotes glycogen storage and cell proliferation in primary human astrocytes. *PLoS One*. 2011;6(6):e21594.
24. García-Cáceres C, et al. Astrocytic insulin signaling couples brain glucose uptake with nutrient availability. *Cell*. 2016;166(4):867–880.
25. Abbott NJ, Rönnbäck L, Hansson E. Astrocyte-endothelial interactions at the blood-brain barrier. *Nat Rev Neurosci*. 2006;7(1):41–53.
26. Bélanger M, Allaman I, Magistretti PJ. Brain energy metabolism: focus on astrocyte-neuron metabolic cooperation. *Cell Metab*. 2011;14(6):724–738.
27. Harada K, Kamiya T, Tsuboi T. Gliotransmitter release from astrocytes: functional, developmental, and pathological implications in the brain. *Front Neurosci*. 2015;9:499.
28. Di Castro MA, et al. Local Ca^{2+} detection and modulation of synaptic release by astrocytes. *Nat Neurosci*. 2011;14(10):1276–1284.
29. Haydon PG, Carmignoto G. Astrocyte control of synaptic transmission and neurovascular coupling. *Physiol Rev*. 2006;86(3):1009–1031.
30. Sakaguchi M, et al. Adipocyte dynamics and reversible metabolic syndrome in mice with an inducible adipocyte-specific deletion of the insulin receptor. *Cell Metab*. 2017;25(2):448–462.
31. Monteggia LM, et al. Brain-derived neurotrophic factor conditional knockouts show gender differences in depression-related behaviors. *Biol Psychiatry*. 2007;61(2):187–197.
32. Palanza P. Animal models of anxiety and depression: how are females different? *Neurosci Biobehav Rev*. 2001;25(3):219–233.
33. Dunlop BW, Nemeroff CB. The role of dopamine in the pathophysiology of depression. *Arch Gen Psychiatry*. 2007;64(3):327–337.
34. Tye KM, et al. Dopamine neurons modulate neural encoding and expression of depression-related behaviour. *Nature*. 2013;493(7433):537–541.
35. Money KM, Stanwood GD. Developmental origins of brain disorders: roles for dopamine. *Front Cell Neurosci*. 2013;7:260.
36. Geiger BM, et al. Evidence for defective mesolimbic dopamine exocytosis in obesity-prone rats. *FASEB J*. 2008;22(8):2740–2746.
37. Deumens R, Blokland A, Prickaerts J. Modeling Parkinson's disease in rats: an evaluation of 6-OHDA lesions of the nigrostriatal pathway. *Exp Neurol*. 2002;175(2):303–317.
38. Maj J, Rogóz Z, Skuza G, Kołodziejczyk K. The behavioural effects of pramipexole, a novel dopamine receptor agonist. *Eur J Pharmacol*. 1997;324(1):31–37.
39. Siuciak JA, Fujiwara RA. The activity of pramipexole in the mouse forced swim test is mediated by D2 rather than D3 receptors. *Psychopharmacology (Berl)*. 2004;175(2):163–169.
40. van Wijngaarden I, Tulp MT, Soudijn W. The concept of selectivity in 5-HT receptor research. *Eur J Pharmacol*. 1990;188(6):301–312.
41. Kreitzer AC, Malenka RC. Striatal plasticity and basal ganglia circuit function. *Neuron*. 2008;60(4):543–554.
42. Jourdain P, et al. Glutamate exocytosis from astrocytes controls synaptic strength. *Nat Neurosci*. 2007;10(3):331–339.
43. Habbas S, et al. Neuroinflammatory TNFα impairs memory via astrocyte signaling. *Cell*. 2015;163(7):1730–1741.
44. Cao X, et al. Astrocyte-derived ATP modulates depressive-like behaviors. *Nat Med*. 2013;19(6):773–777.
45. Paco S, et al. Regulation of exocytotic protein expression and Ca^{2+}-dependent peptide secretion in astrocytes. *J Neurochem*. 2009;110(1):143–156.
46. Araki S, et al. Inhibition of the binding of SNAP-23 to syntaxin 4 by Munc18c. *Biochem Biophys Res Commun*. 1997;234(1):257–262.
47. D'Andrea-Merrins M, Chang L, Lam AD, Ernst SA, Stuenkel EL. Munc18c interaction with syntaxin 4 monomers and SNARE complex intermediates in GLUT4 vesicle trafficking. *J Biol Chem*. 2007;282(22):16553–16566.
48. Jewell JL, et al. Munc18c phosphorylation by the insulin receptor links cell signaling directly to SNARE exocytosis. *J Cell Biol*. 2011;193(1):185–199.
49. Aran V, Bryant NJ, Gould GW. Tyrosine phosphorylation of Munc18c on residue 521 abrogates binding to Syntaxin 4. *BMC Biochem*. 2011;12:19.
50. Arvanitakis Z, Wilson RS, Bienias JL, Evans DA, Bennett DA. Diabetes mellitus and risk of Alzheimer disease and decline in cognitive function. *Arch Neurol*. 2004;61(5):661–666.
51. Goldney RD, Phillips PJ, Fisher LJ, Wilson DH. Diabetes, depression, and quality of life: a population study. *Diabetes Care*. 2004;27(5):1066–1070.
52. Sharma S, Fulton S. Diet-induced obesity promotes depressive-like behaviour that is associated with neural adaptations in brain reward circuitry. *Int J Obes (Lond)*. 2013;37(3):382–389.
53. Sharma AN, Elased KM, Garrett TL, Lucot JB. Neurobehavioral deficits in db/db diabetic mice. *Physiol Behav*. 2010;101(3):381–388.
54. Gupta D, Kurhe Y, Radhakrishnan M. Antidepressant effects of insulin in streptozotocin induced diabetic mice: modulation of brain serotonin system. *Physiol Behav*. 2014;129:73–78.
55. Craft S, et al. Intranasal insulin therapy for Alzheimer disease and amnestic mild cognitive impairment: a pilot clinical trial. *Arch Neurol*. 2012;69(1):29–38.
56. Qiu J, et al. Insulin excites anorexigenic proopiomelanocortin neurons via activation of canonical transient receptor potential channels. *Cell Metab*. 2014;19(4):682–693.
57. Sanchez-Alavez M, et al. Insulin-like growth factor 1-mediated hyperthermia involves anterior hypothalamic insulin receptors. *J Biol Chem*. 2011;286(17):14983–14990.
58. Stouffer MA, et al. Insulin enhances striatal dopamine release by activating cholinergic interneurons and thereby signals reward. *Nat Commun*. 2015;6:8543.
59. Smithers NP, Hodgkinson CP, Cuttle M, Sale GJ. Insulin-triggered repositioning of munc18c on syntaxin-4 in GLUT4 signalling. *Biochem J*. 2008;410(2):255–260.
60. Thurmond DC, Ceresa BP, Okada S, Elmendorf JS, Coker K, Pessin JE. Regulation of insulin-stimulated GLUT4 translocation by Munc18c in 3T3L1 adipocytes. *J Biol Chem*. 1998;273(50):33876–33883.
61. Mauch DH, et al. CNS synaptogenesis promoted by glia-derived cholesterol. *Science*. 2001;294(5545):1354–1357.
62. Corder EH, et al. Gene dose of apolipoprotein E type 4 allele and the risk of Alzheimer's disease in late onset families. *Science*. 1993;261(5123):921–923.
63. Russo SJ, Nestler EJ. The brain reward cir-

cuitry in mood disorders. *Nat Rev Neurosci*. 2013;14(9):609–625.
64. Rajkowska G, Stockmeier CA. Astrocyte pathology in major depressive disorder: insights from human postmortem brain tissue. *Curr Drug Targets*. 2013;14(11):1225–1236.
65. Czéh B, Di Benedetto B. Antidepressants act directly on astrocytes: evidences and functional consequences. *Eur Neuropsychopharmacol*. 2013;23(3):171–185.
66. Kittner H, Franke H, Fischer W, Schultheis N, Krügel U, Illes P. Stimulation of P2Y1 receptors causes anxiolytic-like effects in the rat elevated plus-maze: implications for the involvement of P2Y1 receptor-mediated nitric oxide production. *Neuropsychopharmacology*. 2003;28(3):435–444.
67. Ressler KJ, Nemeroff CB. Role of serotonergic and noradrenergic systems in the pathophysiology of depression and anxiety disorders. *Depress Anxiety*. 2000;12(suppl 1):2–19.
68. Mechoulam R, Parker LA. The endocannabinoid system and the brain. *Annu Rev Psychol*. 2013;64:21–47.
69. Graves SM, Clark MJ, Traynor JR, Hu XT, Napier TC. Nucleus accumbens shell excitability is decreased by methamphetamine self-administration and increased by 5-HT2C receptor inverse agonism and agonism. *Neuropharmacology*. 2015;89:113–121.
70. Yang L, Qi Y, Yang Y. Astrocytes control food intake by inhibiting AGRP neuron activity via adenosine A1 receptors. *Cell Rep*. 2015;11(5):798–807.
71. Chen N, et al. Direct modulation of GFAP-expressing glia in the arcuate nucleus bi-directionally regulates feeding. *Elife*. 2016;5:e18716.